Applied Mathematical Modelling 37 (2013) 9368–9378

Contents lists available at SciVerse ScienceDirect

Applied Mathematical Modelling

journal homepage: www.elsevier.com/locate/apm

Mathematical modeling of solidification process near the inner core boundary of the Earth

D.V. Alexandrov *, A.P. Malygin

Department of Mathematical Physics, Ural Federal University, Ekaterinburg 620000, Russian Federation

ARTICLE INFO

Article history:
Received 1 August 2012
Received in revised form 11 March 2013
Accepted 19 April 2013
Available online 13 May 2013

Keywords:
Mathematical modeling
Solidification
Mushy layer
Inner core boundary
Dendrites

ABSTRACT

Radially symmetric analytic solutions of the heat and mass transfer equations governing convection in the Earth's fluid core are found in terms of deviations from the adiabatic reference state. We demonstrate that an increase of the convective velocity leads to a decrease of the light constituent mass fraction and specific entropy. Where fluid is rising/descending, convective motions decrease/increase the mass fraction and entropy at the inner core boundary (ICB). The influence of convective motions on the thermal fluxes at the core mantle boundary is studied. On the basis of exact solutions we demonstrate that the liquid is supercooled near the ICB. An important point is that an increase in the convective velocity directed to the ICB increases the constitutional supercooling. We show that the anelastic model (AM) can be used only at small supercoolings near the ICB. The most probable solidification scenario "constitutional supercooling and morphological instability" should be described by a mushy layer theory near the ICB and by the AM in the rest region of the fluid outer core. On the basis of dendritic theory and selection mechanisms of crystal growth the dendrite tip radius and interdendritic spacing in the mushy layer at the ICB are determined in the presence of convection.

1. Introduction

It is noteworthy that the Earth's solid core slowly grows as the heavy constituent in the fluid outer core solidifies onto it. This process is connected with the release of latent heat leading to the thermal buoyancy that drives convection in the outer core [1]. The fluid outer core (FOC) can be considered as a binary alloy of iron and some lighter constituent, whose precise chemical composition is unknown. This limitation, to one light constituent, almost certainly oversimplifies a complicated core chemistry, but it suffices since it models a process that is vital to core dynamics, namely gravitational stirring by compositional convection [2]. The realease of light constituent and its displacement by the growing solid phase near the inner core boundary (ICB) would provide a source of compositional buoyancy [3]. Fluid motions within the outer core are influenced by Lorentz, Coriolis and buoyancy forces each of which suppresses possible turbulence [4]. Therefore, convective motions in the outer core can be considered as not turbulent in the first approximation. It is possible that these motions consist of narrow upwellings and broad downwellings [5]. Such fluid flows ($\sim$10 km per year [6]) near the surface of Earth's outer core are sufficient to sustain Earth's magnetic field by means of a mechanism of the geodynamo.

One of the simplest models to calculating the Earth's core dynamics is the Boussinesq approximation. However, the detailed numerical calculations carried out by Glatzmaier and Roberts [7] show that this approach is far from real applications to planets. For this reason, this model was replaced by a more realistic representation of the thermodynamics and convection within the framework of the anelastic approximation. Several particular solutions obtained in [8,9] demonstrate that this

* Corresponding author. Tel.: +7 343 3507541; fax: +7 343 3507429.
E-mail address: Dmitri.Alexandrov@usu.ru (D.V. Alexandrov).

0307-904X/$ - see front matter © 2013 Elsevier Inc. All rights reserved.
http://dx.doi.org/10.1016/j.apm.2013.04.032

approximation is realistic for planet cores. The anelastic approximation of the fluid dynamic equations (see, among others, [10–15]) is based on the assumption that fluid flow velocities are small compared with acoustic velocities. This approach is a good approximation for the Earth's outer core dynamics because acoustic velocities are seven orders of magnitude greater than fluid flow velocities. However, the AM does not take into account the constitutional supercooling near the ICB.

The full system of equations governing convective heat and mass transfer in the Earth's outer core and the geodynamo represents a highly nonlinear system of differential and integral equations (see, among others, [2]). An attempt to find an exact spherically symmetric analytic solution of this problem is presented by Starchenko and Kotel'nikova [16]. Further their solution was corrected in [17]. However, this approach does not consider the formation of a mushy layer near the ICB [18] and convective motions in the FOC representing narrow upwellings and broad downwellings in the vicinity of the phase transition domain [5,19]. The theory under consideration generalizes the AM and the theories of constitutional supercooling and mushy layer formation near the ICB. Our approach demonstrates that the frontal AM with convection leads to the origination of constitutional supercooling in the vicinity of the ICB and, consequently, to the formation of a mushy layer. The Article is organized as follows. A statement of the problem together with analytical solution in the convective approximation is given in Sections 2 and 3. Section 4 deals with the constitutional supercooling appearing near the ICB within the framework of the anelastic approximation. The main parameters of dendrites in the mushy layer in the presence of convection are found in Section 5. Finally, Section 6 gives a summary of our conclusions.

2. The governing equations

The theory of convective heat and mass transfer in the FOC may be conveniently formulated in terms of deviations from a reference state. One of the best models describing this state is the Preliminary Reference Earth Model generally known as "PREM" [20]. This model treats the core as an adiabatic, hydrostatic and spherically-symmetric body (the forces acting on the FOC do not significantly disturb the hydrostatic state). This reference state is maintained by a vigorous convective motions in the FOC. On this basis, the specific entropy $\bar{S}$ and the mass fraction of light constituent $\bar{\xi}$ are independent of spatial variables in the reference state. Since these values depend only on time t, we have

$$\nabla\bar{S} = \nabla\bar{\xi} = 0.$$

The rest time-dependent physical parameters (the density $\bar{\rho}$, temperature $\bar{T}$, gravitational acceleration $\bar{g}$, chemical potential $\bar{\mu}$ and pressure $\bar{p}$) describing the reference state are functions of the spherical radius r, where $r = 0$ at the planet center.

The density of the Earth's core ρ varies from the core mantle boundary (CMB) to the ICB by approximately 20% [21]. These variations lead to the corresponding variations in the adiabatic temperature, gravitational acceleration and chemical potential. Therefore, let us express its spatial variations as the two-parameter polynomial [8]

$$\bar{\rho} = c_1(1 - c_2 r^2). \tag{1}$$

Here the parameters c_1 and c_2 can be determined in terms of the known radii r_{ICB} and r_{CMB}, where the corresponding densities $\bar{\rho}_{\mathrm{ICB}}$ and $\bar{\rho}_{\mathrm{CMB}}$ are set to PREM values (all physical parameters chosen in accordance with PREM values are listed in Table 1). The result is

$$c_1 = \frac{\bar{\rho}_{\mathrm{ICB}}}{1 - c_2 r_{\mathrm{ICB}}^2}, \quad c_2 = \frac{\bar{\rho}_{\mathrm{ICB}} - \bar{\rho}_{\mathrm{CMB}}}{\bar{\rho}_{\mathrm{ICB}} r_{\mathrm{CMB}}^2 - \bar{\rho}_{\mathrm{CMB}} r_{\mathrm{ICB}}^2}.$$

The reference state temperature $\bar{T}$ (adiabatic) and conductive heat flux $\bar{q}$ have the form (hereafter, the prime denotes a radial derivative)

$$\bar{T} = \bar{T}_{\mathrm{ICB}}\left(\frac{\bar{\rho}}{\bar{\rho}_{\mathrm{ICB}}}\right)^{\gamma}, \quad \bar{q} = -c_p \kappa_T \bar{\rho}\frac{d\bar{T}}{dr} = -c_p \kappa_T \bar{\rho}\bar{T}'. \tag{2}$$

Now integrating the gravitational equation

$$(r^2\bar{g})' = 4\pi G\bar{\rho}r^2,$$

we get the gravitational acceleration $\bar{g}(r)$ and potential $\bar{U}_{gp}(r)$

$$\bar{g} = \bar{U}'_{gp} = \frac{c_3}{r^2} + 4\pi G c_1\left(\frac{r}{3} - \frac{c_2 r^3}{5}\right), \tag{3}$$

where c_3 is determined by the reference state gravitational acceleration at the ICB in the form ($\bar{g}_{\mathrm{ICB}} = Gm_{\mathrm{SIC}}/r_{\mathrm{ICB}}^2$, G is the gravitational constant)

$$c_3 = r_{\mathrm{ICB}}^2\left(\bar{g}_{\mathrm{ICB}} - 4\pi G c_1\left(\frac{r_{\mathrm{ICB}}}{3} - \frac{c_2 r_{\mathrm{ICB}}^3}{5}\right)\right).$$

The chemical potential $\bar{\mu}$ of the reference state can be expressed by means of the gravitational potential $\bar{U}_{gp}$ [2,8] as

$$\bar{\mu} = c\left(\bar{U}_{gp}(r) - \bar{U}_{gp}(r_{\mathrm{CMB}})\right), \tag{4}$$

where $c = -0.6$ and $\bar{\mu}$ has been set to zero at the CMB [8].

Table 1
Parameters used for calculations.

Density, $\bar{\rho}_{\mathrm{ICB}}$	12166 kg m^{-3}
Density, $\bar{\rho}_{\mathrm{CMB}}$	9903 kg m^{-3}
Density, ρ_{SIC}	12764 kg m^{-3}
Specific thermal flux, q_S	$1.4 \cdot 10^{-2}$ W m^{-2}
Temperature, $\bar{T}_{\mathrm{ICB}}$	5300 K
Radius, r_{ICB}	$1222 \cdot 10^{3}$ m
Radius, r_{CMB}	$3480 \cdot 10^{3}$ m
Mass, m_{SIC}	$9.839 \cdot 10^{22}$ kg
Light constituent diffusivity, κ_ξ	2 m^2 s^{-1}
Entropy diffusivity, κ_S	2 m^2 s^{-1}
Temperature diffusivity, κ_T	$5 \cdot 10^{-6}$ m^2 s^{-1}
Grüneisen parameter, γ	1.35
Light constituent jump, $\Delta\xi$	0.065
Entropy jump, ΔS	190 J kg^{-1} K^{-1}
Freezing number, f_ξ	70
Freezing number, f_S	33
Rate of light constituent change, $\dot{\bar{\xi}}$	$5 \cdot 10^{-20}$ s^{-1}
Rate of entropy production, $\dot{\bar{S}}$	-10^{-16} W kg^{-1} K^{-1}
Specific heat, c_p	840 J kg^{-1} K^{-1}
Temperature gradient, G_l	$-10.9 \cdot 10^{-4}$ K
Temperature gradient, G_s	$-1.7 \cdot 10^{-4}$ K
Thermal conductivity, k_l	63 J m^{-1} K^{-1} s^{-1}
Thermal conductivity, k_s	79 J m^{-1} K^{-1} s^{-1}
Latent heat, L_V	$6.84 \cdot 10^{9}$ J m^{-3}
Partition coefficient, k	0.25
Slope of the liquidus, m_P	$9 \cdot 10^{-9}$ K Pa^{-1}
Acceleration of gravity, g	4.4 m s^{-2}
Concentration of light element in outer core, C_∞	0.01

The reference state pressure $\bar{p}$ is determined by integrating the hydrostatic equation

$$\bar{p} = p_{\mathrm{ICB}} - \int_{r_{\mathrm{ICB}}}^{r} \bar{\rho}\bar{g}dr,$$

where $p(r = r_{\mathrm{ICB}})$ corresponds to the PREM value.

Let us describe convective motions in the Earth's outer core as a perturbation of the reference state in the form $\bar{S} + S,\ \bar{\xi} + \xi,\ \bar{p} + p,\ \mathbf{V}$ (variables without the bar designate these perturbations). The governing equations for perturbations in a frame of reference rotating at constant angular velocity $\boldsymbol{\Omega}$ have the form [2,16]

$$\nabla(\bar{\rho}\mathbf{V}) = 0, \tag{5}$$

$$\frac{\partial \mathbf{V}}{\partial t} + (\mathbf{V}\nabla)\mathbf{V} + 2\boldsymbol{\Omega} \times \mathbf{V} = -\frac{\nabla p}{\bar{\rho}} + \kappa_V \nabla^2 \mathbf{V} + A\mathbf{e}_r, \tag{6}$$

$$\nabla(\kappa_\xi \bar{\rho} \nabla \xi) = \bar{\rho}\left(\frac{\partial \xi}{\partial t} + (\mathbf{V}\nabla)\xi + \dot{\bar{\xi}}\right), \tag{7}$$

$$\nabla(\kappa_S \bar{\rho}\bar{T}\nabla S) = \bar{\rho}\bar{T}\left(\frac{\partial S}{\partial t} + (\mathbf{V}\nabla)S + \dot{\bar{S}}\right) + \frac{1}{r^2}\left(r^2\bar{q}\right)' - \kappa_\xi \bar{\rho}\bar{\mu}'\xi', \tag{8}$$

where $\boldsymbol{\Omega} = \Omega\mathbf{e}_z,\ \dot{\bar{\xi}} = d\bar{\xi}/dt,\ \dot{\bar{S}} = d\bar{S}/dt,\ A = -S\bar{T}' - \xi\bar{\mu}',\ \mathbf{e}_r$ and $\mathbf{e}_z$ are the unit vectors of the spherical coordinate system. The aforementioned anelastic equations describe mass conservation (5), momentum conservation (6), composition (7) and heat (8). Here A is the radial acceleration caused by the Archimedean force responsible for the convection rate. The negative heat flux $(r^2\bar{q})'/r^2$ in expression (8) represents the deviation from the adiabatic specific radiation heat determined as $\bar{q} = -\kappa_T c_p \bar{\rho}\bar{T}'$. The cooling term $\bar{\rho}\bar{T}\dot{\bar{S}}$ compensates this outflow and maintains the reference state. Small viscosity terms in (8) are neglected. In the case of convection, the viscosity κ_V and diffusivities of light constituent (κ_ξ) and entropy (κ_S) are expressed in terms of turbulent tensors. These transfer coefficients can be estimated close to $\sim$2 m^2/s [2,22] whereas the temperature diffusivity is of the order of 10^{-6} m^2/s [21].

The growth rate of the local inner core radius R is determined by means of the freezing numbers of light constituent f_ξ and specific entropy f_S as

$$\frac{\partial R}{\partial t} = -r_{\mathrm{ICB}}\left(\frac{f_S}{c_p}\frac{\partial S}{\partial t} + f_\xi \frac{\partial \xi}{\partial t}\right). \tag{9}$$

The crystallization process at the ICB leads to the corresponding boundary conditions for ξ and S. The growth rate of the inner core radius is proportional to the local fluxes of light constituent and entropy at the ICB [2]

$$\frac{\partial R}{\partial t} = -\frac{\kappa_S \bar{\rho}_{\mathrm{ICB}}}{\Delta S \rho_{\mathrm{SIC}}}(S')_{\mathrm{ICB}} = -\frac{\kappa_\xi \bar{\rho}_{\mathrm{ICB}}}{\Delta \xi \rho_{\mathrm{SIC}}}(\xi')_{\mathrm{ICB}}, \quad r = r_{\mathrm{ICB}}, \tag{10}$$

where the jumps of entropy ΔS and light constituent $\Delta\xi$ on passing the phase transition boundary are given in Table 1.

The flux of light constituent should be absent on the CMB whereas the flux of entropy is expressed in terms of the specific thermal flux q_S on the CMB, i.e.

$$\xi' = 0, \quad S' = -\frac{q_S}{\kappa_S \bar{T}\bar{\rho}_{\mathrm{CMB}}}, \quad r = r_{\mathrm{CMB}}. \tag{11}$$

The nonadiabatic thermal flux $q - \bar{q}$ is the difference between the total thermal flux q and the flux $\bar{q}$ caused by the thermal conductivity at the CMB. The total thermal flux coming from the Earth's core is unknown. Therefore, even the sign of the mean value $q - \bar{q}$ designated by q_S is also unknown ($q_S = \pm 10^{-2}$ W/m^2 in accordance with estimates given by Glatzmaier and Roberts [9]).

3. Spherically symmetric solution with convection

Let us seek for a spherically symmetric solution of convective Eqs. (5)–(8) depending only on r. In this case, Eqs. (5), (7) and (8) become

$$\left(r^2 \bar{\rho} V_r\right)' = 0, \tag{12}$$

$$\frac{\kappa_\xi}{r^2\bar{\rho}}\left(r^2\bar{\rho}\xi_r'\right)' = \dot{\xi}_r + \dot{\bar{\xi}} + V_r \xi_r', \tag{13}$$

$$\frac{\kappa_S}{r^2\bar{\rho}\bar{T}}\left(r^2\bar{\rho}\bar{T}S_r'\right)' = \dot{S}_r + \dot{\bar{S}} + V_r S_r' + \frac{1}{r^2\bar{\rho}\bar{T}}\left(r^2\bar{q}\right)' - \frac{\kappa_\xi}{\bar{T}}\bar{\mu}'\xi_r', \tag{14}$$

where $\dot{\xi}_r = \partial\xi_r/\partial t$, $\dot{S}_r = \partial S_r/\partial t$, ξ_r and S_r designate the radially symmetric solutions. Eq. (6) is required for the determination of pressure perturbations p.

Expressions (9) and (10) give the following boundary conditions at $r = r_{\mathrm{ICB}}$

$$\frac{\kappa_S \bar{\rho}_{\mathrm{ICB}}}{\Delta S \rho_{\mathrm{SIC}} r_{\mathrm{ICB}}} S_r' = \frac{\kappa_\xi \bar{\rho}_{\mathrm{ICB}}}{\Delta\xi \rho_{\mathrm{SIC}} r_{\mathrm{ICB}}}\xi_r' = \frac{f_S}{c_p}\dot{S}_r + f_\xi \dot{\xi}_r. \tag{15}$$

The boundary conditions for S_r and ξ_r at $r = r_{\mathrm{CMB}}$ follow from expressions (11).

Integration of Eq. (12) gives

$$V_r = \frac{c_0}{r^2\bar{\rho}(r)}, \tag{16}$$

where c_0 is a constant.

The spherically symmetric solution is the best approximation of equations governing convection in Earth's core in those regions of the FOC where fluid is rising or descending (see, among others, Fig. 2 in Ref. [9]). Therefore, introducing the mean velocity in the upwelling (downwelling) convective plume

$$\bar{U} = \frac{1}{r_{\mathrm{CMB}} - r_{\mathrm{ICB}}}\int_{r_{\mathrm{ICB}}}^{r_{\mathrm{CMB}}} V_r(r)dr,$$

we find the constant of integration

$$c_0 = \bar{U}(r_{\mathrm{CMB}} - r_{\mathrm{ICB}})\left[\int_{r_{\mathrm{ICB}}}^{r_{\mathrm{CMB}}} \frac{dr}{r^2\bar{\rho}(r)}\right]^{-1}.$$

Seeking the mass fraction of light constituent and the specific entropy as a sum of functions $\xi_r = \xi_{r1}(r) + \xi_{r2}(t)$ and $S_r = S_{r1}(r) + S_{r2}(t)$ (here ξ_{r1}, S_{r1} and ξ_{r2}, S_{r2} represent arbitrary functions of r and t respectively) and taking into account expressions (11) and (16), we come to the spherically symmetric solution of convective Eqs. (13) and (14)

$$\xi_r = \xi_{\mathrm{CMB}} + \frac{A}{\kappa_\xi}\int_{r_{\mathrm{CMB}}}^{r} \frac{I_1(r)dr}{r^2\bar{\rho}}, \tag{17}$$

$$S_r = S_{CMB} + \int_{r_{CMB}}^{r} \frac{BI_2 + I_3 - r_{CMB}^2 q_S/f_2}{\kappa_S r^2 \bar{\rho}\bar{T}} dr, \tag{18}$$

where

$$I_1(r) = f_1^{-1}(r) \int_{r_{CMB}}^{r} r^2 \bar{\rho}(r) f_1(r) dr, \quad I_2(r) = f_2^{-1}(r) \int_{r_{CMB}}^{r} r^2 \bar{\rho}(r) \bar{T}(r) f_2(r) dr,$$

$$I_3(r) = f_2^{-1}(r) \int_{r_{CMB}}^{r} H(r) r^2 \bar{\rho}(r) \bar{T}(r) f_2(r) dr,$$

$$H(r) = \frac{1}{r^2 \bar{\rho}\bar{T}} \left(r^2 \bar{q}\right)' - \frac{\kappa_\xi}{\bar{T}} \bar{\mu}' \xi_r',$$

$$f_1(r) = \exp\left(-\int_{r_{CMB}}^{r} V_r dr/\kappa_\xi\right), \quad f_2(r) = \exp\left(-\int_{r_{CMB}}^{r} V_r dr/\kappa_S\right).$$

Substituting solutions (17) and (18) into the boundary conditions (15), we come to the following expressions for A and B

$$A = \frac{I_2(r_{ICB})[\dot{\bar{S}} + (c_p/f_S) f_\xi \dot{\bar{\xi}}] + I_4(r_{ICB}) - q_S r_{CMB}^2/f_2(r_{ICB})}{I_5(r_{ICB}) + \Delta S I_1(r_{ICB}) \bar{T}(r_{ICB})/\Delta\xi - M},$$

$$M = \frac{c_p I_2(r_{ICB})}{f_S} \left[\frac{I_1(r_{ICB})}{\Delta\xi r_{ICB}^3 \rho_{SIC}} - f_\xi\right], \quad B = \dot{\bar{S}} + \frac{c_p}{f_S} f_\xi \dot{\bar{\xi}} + \frac{A c_p}{f_S} \left[\frac{I_1(r_{ICB})}{\Delta\xi r_{ICB}^3 \rho_{SIC}} - f_\xi\right],$$

$$I_4(r) = f_2^{-1}(r) \int_{r_{CMB}}^{r} \left(r^2 \bar{q}\right)' f_2(r) dr, \quad I_5(r) = f_2^{-1}(r) \int_{r_{CMB}}^{r} \bar{\mu}' I_1(r) f_2(r) dr.$$

The boundary values ξ_{CMB} and S_{CMB} follow from the FOC integrals [8]

$$\int_{FOC} \bar{\rho}(r) \xi_r dV = 4\pi \int_{r_{ICB}}^{r_{CMB}} \bar{\rho}(r) \xi_r r^2 dr = 0,$$

$$\int_{FOC} \bar{\rho}(r) S_r dV = 4\pi \int_{r_{ICB}}^{r_{CMB}} \bar{\rho}(r) S_r r^2 dr = 0.$$

After integration, we have

$$\xi_{CMB} = \frac{A}{\kappa_\xi} \int_{r_{ICB}}^{r_{CMB}} \frac{I_1(r) F(r) dr}{r^2 \bar{\rho}(r) F(r_{CMB})}, \quad F(r) = \frac{r^3 - r_{ICB}^3}{3} - \frac{c_2 (r^5 - r_{ICB}^5)}{5},$$

$$S_{CMB} = \int_{r_{ICB}}^{r_{CMB}} \frac{BI_2(r) + I_3(r) - r_{CMB}^2 q_S/f_2(r)}{\kappa_S r^2 \bar{\rho}(r) \bar{T}(r)} \frac{F(r)}{F(r_{CMB})} dr.$$

Now pressure perturbations p can be easily found by integration of Eq. (6). Note that expressions (17) and (18) are independent of time if $\dot{\bar{\xi}}$, $\dot{\bar{S}}$, ξ_{CMB}, S_{CMB} and q_S are constants [2,8,9,16,17].

Let us especially emphasize that expression (16) represents an approximation of the fluid velocity in the FOC except those regions where horizontal flows become comparable with vertical flows. Although we do not consider the hydrodynamics in these boundary layers, expressions (17) and (18) lead to an adequate physical behavior of obtained solutions near the CMB. This is due to the fact that the light constituent mass fraction ξ_r and the specific entropy S_r are dependent on V_r only by means of functions $f_1(r)$ and $f_2(r)$ representing vanishing integrals at $r = r_{CMB}$. This result follows from equations (13) and (14) integrated in the case of arbitrary function $V_r(r)$.

Analytical distributions (17) and (18) describe the convective solution of spherically symmetric problem as well as the case of a motionless fluid ($\bar{U} = 0$).

Figs. 1 and 2 show the spherically symmetric parts of ξ and S (physical parameters used for calculations (see Table 1) correspond to previous studies [8,9,16]). An increase in the convective velocity $\bar{U}$ leads to a decrease of perturbations of the light constituent mass fraction and specific entropy. In the absence of convective motions ($\bar{U} = 0$) the mass fraction ξ_r increases at the ICB due to the impurity displacement by the growing solid phase. Where fluid is rising ($\bar{U} > 0$), convective motions decrease this function at the ICB and where fluid is descending ($\bar{U} < 0$), ξ_r increases near the ICB due to the impurity flux from the FOC. The same influence of convection on perturbations of the specific entropy S_r is illustrated in Fig. 2. Note that the spherically symmetric solution shown in Figs. 1 and 2 differs from the numerical magnetohydrodynamic (MHD) simulations [8,9] by only several times despite the fact that the energy of the magnetic field in these papers, which we neglected, was several orders of magnitude greater than the energy of the velocity field. Therefore, the solution under consideration should

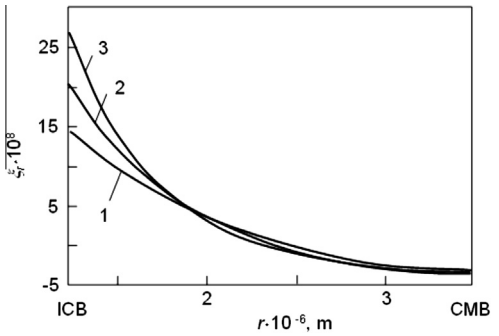

Fig. 1. The radial distribution of the spherically symmetric perturbations ξ_r (relative to the reference state) of the light constituent mass fraction for different mean velocities $\bar{U} = 10^{-6}$ m/s (1), $\bar{U} = 0$ m/s (2), $\bar{U} = -10^{-6}$ m/s (3).

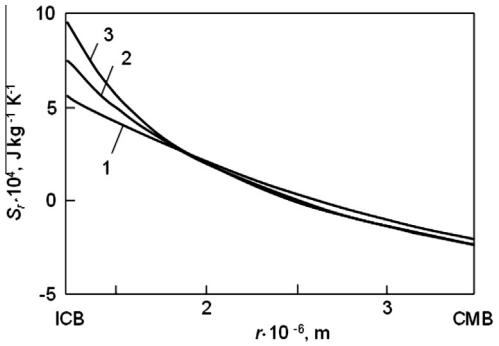

Fig. 2. The radial distribution of the spherically symmetric perturbations S_r (relative to the reference state) of the specific entropy for different mean velocities $\bar{U} = 10^{-6}$ m/s (1), $\bar{U} = 0$ m/s (2), $\bar{U} = -10^{-6}$ m/s (3).

determine the sources of not only nonmagnetic but also MHD convection. This is also confirmed by MHD estimates presented by Anufriev and Cupal [22]: they have shown that the characteristic amplitude of the magnetic field relates more to the axisymmetrical part of the MHD equations. Therefore, the present analytical distributions can also be used as test solutions for numerical calculations of the full MHD equations.

Let us now express the growth rate of the solid inner core (SIC) from the boundary conditions (10). Substitution ξ_r from (17) into (10) gives

$$\dot{R} = -\frac{AI_1(r_{\mathrm{ICB}})}{\Delta\xi\rho_{\mathrm{SIC}}r_{\mathrm{ICB}}^2}. \tag{19}$$

Fig. 3 shows that an increase of the mean fluid velocity $\bar{U}$ leads to a decrease of the specific thermal flux q_S at a critical point $q_S = q_C$ responsible for the positive growth rate $\dot{R} > 0$ at $q_S > q_C$ ($q_C = q_S$ at $\dot{R} = 0$). In other words, the growth condition $\dot{R} > 0$ is not satisfied when $\bar{q} > q - q_C$. When the total thermal flux q is greater than $\bar{q} + q_C$, the present diffusion solution with convection can itself describe the growth process at the ICB. Let us especially note that the critical flux $q_C < 0$ for all values of the fluid velocity $\bar{U}$ illustrated in Fig. 3. Considering that the upper limit of the absolute value $|\bar{U}|$ is 10^{-4} m/s [4], we conclude that $q_C < 0$ for all possible convective flows in the FOC. What this means is the total heat flux q is greater than the adiabatic flux $\bar{q}$ when $q_S > 0$ and $q_C + \bar{q} < q < \bar{q}$ when $q_C < q_S < 0$. It is easy to see that the case of descending fluid (at a high velocity $\sim -10^{-4}$ m/s) will most likely be described by the inequality $q > \bar{q}$. The opposite case when fluid is rising (at a high velocity $\sim 10^{-4}$ m/s) corresponds to sufficiently small rates $\dot{R}$ due to small values of the constitutional supercooling near the ICB. Note that the growth rate $\dot{R}$ is practically linear function of the specific thermal flux q_S for different fluid velocities. Let us also emphasize that the growth rate $\dot{R}$ increases with decreasing $\bar{U} < 0$. This is caused by the light constituent flux directed to the ICB, which increases the constitutional supercooling near the SIC. This conclusion is in agreement with the morphological stability analysis of the ICB [18], where two possible solidification scenarios have been found: "constitutional supercooling and morphological stability" and "constitutional supercooling and morphological instability" corresponding to the slurry and mushy layer theories [18,23–26]. If the total heat flux at the ICB is larger than the adiabatic heat flux near the ICB and the total heat flux near the CMB is less than the adiabatic heat flux there [21] then a point at which these fluxes coincide moves to the CMB with decreasing the convective velocity $\bar{U} \sim -10^{-4}$ m/s ($q_C \to -0$, Fig. 3).

An important point is that the growth rate of the inner core is greater in a descending part (Fig. 3). This is because that this part of the ICB becomes colder due to a cold convective fluid flux going to the ICB from the FOC. Those parts of the ICB where

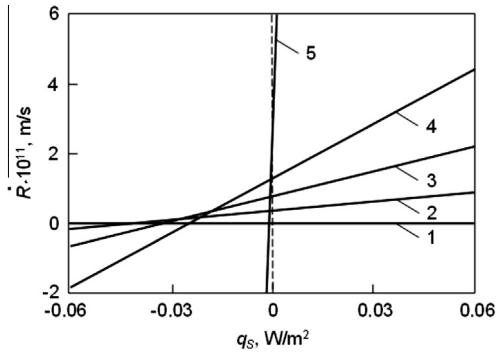

Fig. 3. The growth rate of the SIC boundary as a function of the specific thermal flux for different mean velocities $\bar{U} = 10^{-4}$ m/s (1), $\bar{U} = 10^{-6}$ m/s (2), $\bar{U} = 0$ m/s (3), $\bar{U} = -10^{-6}$ m/s (4), $\bar{U} = -10^{-4}$ m/s (5); line 1 is above zero. Region $\dot{R} < 0$ is shown only to demonstrate the influence of q_S and $\bar{U}$ on the growth rate.

fluid rises represent the hotter regions of heat removal from the ICB to the FOC. As a result, the growth rate of these parts calculated on the basis of the locally planar model is smaller than the rate in descending regions. This difference is the reason of morphological instability and dendritic growth in the supercooled regions corresponding to those parts of the ICB where a cold fluid descends. This physical bevavior is similar to solidification processes met in crystal growth and metallurgy [19,27–29].

4. Constitutional supercooling and the anelastic approximation

Let us assume that the impurity is initially distributed uniformly in the FOC in the vicinity of the ICB, whereas the temperature gradients are such that the solidification front moves at constant velocity V and temperature of the melt is higher than the phase transition temperature. As the partition coefficient k equal to the ratio of concentration in the solid and liquid phase to both sides of the crystallization front is smaller than unity, the movement of the phase interface will be accompanied by displacement of the impurity by the front and its removal into the melt by the diffusion and convection mechanisms. As a result, the impurity will be accumulated directly upstream of the front. This will increase the temperature of phase transition in the melt with increasing distance from the phase interface. The phase transition temperature at the front itself drops according to the phase diagram. These mechanisms lead to some steady distribution of the impurity, phase transition temperature T_p and of the temperature in the melt T. If the temperature gradient G_L in the melt at the front is lower than or equal to the gradient G of the phase transition temperature, then a supercooled region will form upstream of the front.

In the case under consideration the phase transition temperature depends on both the solute concentration (mass fraction of light constituent $\Xi = \bar{\xi} + \xi$) and the pressure $P = \bar{p} + p$. Designating the liquidus (m_C) and Clapeyron (m_P) slopes as $m_C = (\partial T_p/\partial \Xi)_p < 0$ and $m_P = (\partial T_p/\partial P)_\Xi > 0$, we get the supercooling criterion at the ICB

$$G_L \leqslant G = m_P G_P + m_C G_C, \tag{20}$$

where G_P and G_C stand for the pressure and concentration gradients.

It is known from thermodynamics that the entropy differential in the FOC can be written in the form [2,21]

$$d(\bar{S} + S) = \frac{c_p}{T} dT - \frac{\alpha}{\rho} dP + \frac{h^\xi}{T} d\Xi,$$

where α is the coefficient of thermal expansion and h^ξ is the heat of reaction.

Dividing this equation by dr and taking into account that $\nabla\bar{S} = \nabla\bar{\xi} = 0$ in the reference state, we come to the following expressions at the phase transition interface (ICB)

$$\bar{g}_L = \frac{\alpha \bar{T}_{\mathrm{ICB}}}{c_p \bar{\rho}_{\mathrm{ICB}}} \bar{g}_P = m_P \bar{g}_P, \tag{21}$$

$$g_L - m_P g_P - m_C g_\xi = \frac{\bar{T}_{\mathrm{ICB}}}{c_p} g_S < 0, \tag{22}$$

where $m_C = -h^\xi/c_p$ and all gradients are presented in the form of reference values (barred variables) and perturbations as

$$\nabla T = G_L = \bar{g}_L + g_L, \quad \nabla P = G_P = \bar{g}_P + g_P, \quad \nabla \Xi = G_C = \nabla\bar{\xi} + g_\xi, \quad \nabla S = g_S.$$

Expression (21) shows that inequality (20) becomes equality, i.e. that the adiabatic reference state describes the frontal solidification scenario with minimum supercooling. Substituting expression (21) into (20), we rewrite the condition of constitutional supercooling for perturbations in the form

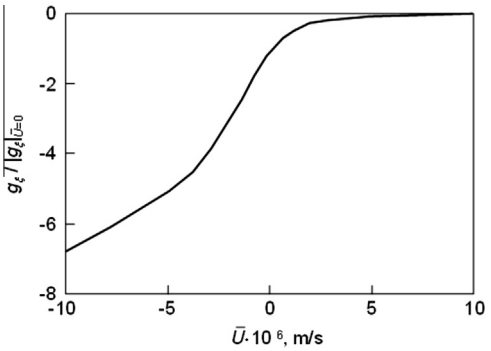

Fig. 4. The relative concentration gradient at the ICB vs. the mean fluid velocity.

$$g_L - m_P g_P - m_C g_\zeta \leqslant 0. \tag{23}$$

Inequality (23) is always true in the case of spherically symmetric solutions because $\bar{T}_{\mathrm{ICB}} g_S / c_p = \bar{T}_{\mathrm{ICB}} S_r' / c_p < 0$ at the ICB (see expression (22) and Fig. 2). In other words, the well-known anelastic frontal model under consideration demonstrates that the liquid is always supercooled near the ICB even in the non-convecting case. An important point is that an increase in the convective velocity directed to the ICB increases the constitutional supercooling in accordance with analytical solutions shown in Figs. 2 and 4. The reason is that the impurity concentration near the ICB undergoes only a small rise due to its flux from the FOC to the ICB transferred by a cold fluid when $\bar{U} < 0$. In the opposite case $\bar{U} > 0$, in regions where fluid rises it is hotter because these convective zones represent the channels of heat removal from the ICB to the FOC.

As the melt near the ICB is always supercooled there are two possible solidification scenarios: "constitutional supercooling and morphological stability" and "constitutional supercooling and morphological instability" [18]. These regimes are completely determined by convective motions at the ICB. The first case is described by the planar solidification front or the slurry layer model, whereas the second case corresponds to the formation of a mushy layer filled by dendrite structures [18]. In accordance with estimates presented by Fearn et al. [30] this dendrite region in which phase transition takes place may extend throughout the FOC.

It is significant that only the first of these scenarios can be described by means of the AM at small supercoolings. When supercooling is large enough the AM approach with corresponding boundary conditions cannot be used in the ICB region. This approach should be modified to take into account possible mushy layer effects near the ICB. In other words, the most probable scenario "constitutional supercooling and morphological instability" should be described by a mushy layer theory [18,19,23,24,31] near the ICB and by the AM theory [2,21] in the rest region of the FOC with new boundary conditions imposed at the mushy layer – FOC interface. Such model is needed to improve the geodynamo simulations [8,9].

Note that the theoretical analysis [32] shows that solidification process at the ICB most likely proceeds by formation of a mushy layer because of the difficulty to supply enough nuclei to feed a slurry layer. The slurry layer solidification scenario requires a sufficiently large supercooling at the ICB to initiate the nucleation process. If this is really the case, one can use the theoretical approach developed previously [18,26,32,33]. Below we consider the growth of dendritic structures in the mushy layer near the ICB developing at small supercoolings.

5. Dendritic growth near the ICB

Let us now estimate the main parameters of this supercooled (mushy) layer in the presence of convection. Its thickness highly dependent on the velocity of convection is a few hundred of meters [18]. This layer is filled with dendrites and similar structures which determine the mushy layer permeability. In its turn, the permeability is a necessary parameter to study the hydrodynamics in porous media. It is known that the mushy layer permeability is roughly proportional to the square of the primary dendrite spacing λ_1 [34]. In the case of stationary state and axisymmetric dendrite tip, we have [35]

$$\lambda_1 = \sqrt{\frac{2\pi\rho}{a(\partial\varphi/\partial r)_{\mathrm{ICB}}}}, \tag{24}$$

where ρ is the dendrite tip radius, φ is the solid fraction, $a = 1$ and $a \approx 0.86$ for a cubic and hexagonal dendritic array respectively. Let us now calculate ρ and φ in the presence of convection.

One of the theoretically and practically important problems consists in obtaining stable crystallization mode of the growing dendrite. After establishing robust stable conditions for the dendritic tip growing into a one-component stagnant liquid [36–39], these were extended to the one-component dendritic growth under forced flow [40,41], to the binary dendritic growth in a stagnant media [42] and to the binary dendritic growth under forced flow [43,44]. The main predictions of these theories are (i) that the crystal shape remains parabolic near the tip of the dendrite, (ii) that the product $\rho^2 V = \mathrm{const}$ (V

stands for the growth velocity), which is known to be valid for dendritic growth without flow remains true in the presence of an external flow, and (iii) that $\rho^2 V$ does not depend on the transverse component of the flow and increases linearly with the longitudinal component V_r of the flow as [43]

$$\rho^2 V = 2\frac{d_0 D}{\sigma}\left(1 + \frac{\chi d_0}{D} V_r\right) \tag{25}$$

for different concentrations of impurity of the order of 10^{-2} typical for the ICB conditions. Here d_0 is the capillary length, D is the chemical diffusion coefficient, σ and χ are two numerical constants, estimated as 0.032 and 5300 [43]. Contrary to the purely diffusive expression for the dendrite tip radius [35], expression (25) takes into account the influence of convection. Taking into consideration that $|V_r|$ is less than 10^{-4} m/s [4], V ranges from $6 \cdot 10^{-12}$ m/s to $2 \cdot 10^{-11}$ m/s [35], $D = 10^{-9}$ m^2/s and $d_0 \sim 10^{-9}$ to 10^{-10} m, we obtain that the dendrite tip radius varies twofold from ~0.5 mm to ~1 mm. These estimates are in good agreement with $\rho \sim 1$ mm found in Ref. [35] for a stagnant fluid.

Let us now express the derivative of the solid fraction with respect to r entering in Eq. (24). To do this would require the heat balance condition at the ICB

$$k_s G_s - L_V(1 - \varphi_{\mathrm{ICB}})V = k_{sl}(\varphi_{\mathrm{ICB}})\frac{dT}{dr} = k_{sl}(\varphi_{\mathrm{ICB}})G_l, \tag{26}$$

the temperature gradient dT/dr in the mushy layer known from the phase diagram

$$\frac{dT}{dr} = m_C \frac{dC}{dr} + m_P G_P \tag{27}$$

and the Scheil expression [45] connecting the impurity concentration C and the solid fraction φ in the phase transition domain

$$C(\varphi) = C_\infty (1 - \varphi)^{k-1}, \tag{28}$$

where $k_{sl}(\varphi_{\mathrm{ICB}}) = k_l(1 - \varphi_{\mathrm{ICB}}) + k_s\varphi_{\mathrm{ICB}}$, k_s and k_l are the thermal conductivities in the solid and liquid phases, φ_{ICB} is the solid fraction φ at the ICB, L_V is the latent heat, G_s is the temperature gradient in the inner core, G_P is the pressure gradient in the outer core near the ICB, m_C and m_P are the concentration and pressure liquidus slopes, C_∞ is the impurity concentration in the liquid far from the ICB and k is the partition coefficient. Eq. (28) shows that the solid fraction at the boundary between the mushy layer and the FOC turns to zero. Combining expressions (26)–(28) we have

$$\left(\frac{d\varphi}{dr}\right)_{\mathrm{ICB}} = \frac{k_s G_s - L_V V(1 - \varphi_{\mathrm{ICB}}) - k_{sl}(\varphi_{\mathrm{ICB}})m_P G_P}{k_{sl}(\varphi_{\mathrm{ICB}})m_C C_\infty (1 - k)(1 - \varphi_{\mathrm{ICB}})^{k-2}}, \tag{29}$$

where $G_P = -\bar{\rho}_{\mathrm{ICB}} g$ and φ_{ICB} can be found in terms of the temperature gradient G_l in the outer core at the ICB

$$\varphi_{\mathrm{ICB}} = \frac{k_s G_s - k_l G_l - L_V V}{(k_s - k_l)G_l - L_V V}.$$

Note that the solid fraction profile in the mushy layer $\varphi(r)$ is found in Ref. [18] in terms of its inverse function. We refer the reader to this paper for further discussion.

Now substitution of expressions (25) and (29) into (24) completely determines the interdendritic spacing in the mushy layer. Fig. 5 shows that increasing the fluid velocity near the ICB increases λ_1. However, the liquidus slope has a more significant influence on this parameter: λ_1 ranges from ~3 m to ~40 m. If the value $m_C \sim -10^4$ K is more probable than $m_C \sim -10^2$ K [32] then the interdendriting spacing at the ICB is of the order of 30–40 m in the presence of convection. This

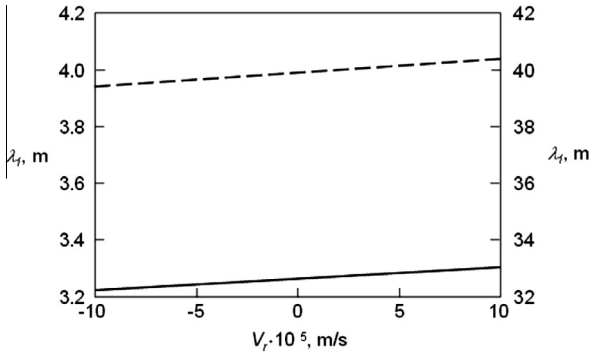

Fig. 5. Interdendritic spacing λ_1 as a function of the fluid velocity V_r in the mushy layer near the ICB for different solidification rates $V = 0.9 \cdot 10^{-11}$ m/s (solid line) and $V = 1.2 \cdot 10^{-11}$ m/s (dashed line) and liquidus slopes $m_c = -10^2$ K (scale of values on the left) and $m_c = -10^4$ K (scale of values on the right). Physical parameters used for calculations are listed in Table 1, $a = 0.86$.

value is three/four times larger than the corresponding value found in [35] on the basis of approximate estimates of $(\partial\varphi/\partial r)_{\mathrm{ICB}}$ for a stagnant fluid and it is significantly smaller than estimate of a few hundred meters obtained on the basis of scaling laws in Ref. [46].

6. Conclusion

It is likely that the mushy layer near the ICB has a very similar structure as in the case of binary alloy solidification process [19]: this layer represents broad areas where fluid is descending from the FOC divided by narrow areas called by chimneys where fluid is rising. In those regions where fluid rises, its flux dissolves the dendrites and forms a chimney in the mushy layer. Most parts of regions where fluid is descending have a radial symmetry and consequently they can be described by means of the radially symmetric approach under consideration. This theory is in agreement with the linear morphological stability analysis in the presence of convection recently developed in Ref. [18]: the instability domain exists for $V_r < 0$ where fluid is descending. The physical reason of morphological instability is that the ICB is supercooled where $V_r < 0$. This conclusion follows from the AM equations under consideration and from the stability analysis [18]. Most likely these unstable regions of the ICB represent mushy layers filled by growing dendrites whose main parameters are found in the present study in the case of a forced flow.

Let us now summarize in conclusion the main steps and aspects of the theory under consideration.

(i) The radially symmetric solutions for perturbations of the anelastic equations [2,21] are found analytically in the presence of convection. These solutions probably represent the sources of MHD convection in the FOC.
(ii) The growth rate of the SIC boundary is theoretically found as a function of the specific thermal flux and mean fluid velocity. This rate is nearly liner function of the specific thermal flux for different fluid velocities. The regions of the SIC where fluid is descending/rising correspond to large/small growth rates. As this takes place, the growth rate of the SIC increases with increasing the absolute value of the descending fluid velocity due to the effect of increased constitutional supercooling near the ICB.
(iii) Under these conditions our solutions show that the descending fluid is always supercooled near the ICB. These supercooled regions of unstable growth of the SIC represent mushy layers most likely filled by growing dendrites. What this means is the AM approach, generally speaking, is valid only at small supercoolings near the ICB where the SIC boundary represents the solidification front. The most probable scenario at the unstable SIC boundary where supercooled fluid is descending should be described by a mushy layer theory in the vicinity of the ICB and by the AM in the rest region of the FOC.
(iv) The main parameters characterizing dendritic growth near the ICB are determined in the presence of convective flow. The dendrite tip radius varies from $\sim$0.5 mm to $\sim$1 mm when the growth rate ranges from $6 \cdot 10^{-12}$ m/s to $2 \cdot 10^{-11}$ m/s. The interdendritic spacing therewith becomes of the order of 30–40 m in the presence of convection.
(v) Possible arrangement of the mushy layer at the ICB is predicted. It represents broad regions where fluid is descending to the SIC divided by narrow chimneys where fluid is rising. The mushy layers with dendrites therewith are located in the first regions, whereas the second ones represent the chimneys where fluid dissolves dendrites and where the SIC boundary remains locally planar [47,48].

Thus, a better model of heat and mass transfer equations and boundary conditions at the ICB including the AM aproximation and the convective mushy layer theory with chimney formation is needed to describe the evolution of the ICB and the magnetohydrodynamics in the FOC more precisely.

Acknowledgements

We are grateful for partial support from the Federal Target Program "Scientific and Academic – Teaching Staff of Innovative Russia" in 2009–2013 and the Russian Foundation for Basic Research (Project No. 11-01-00137).

References

[1] J. Verhoogen, Heat balance of the Earth's core, Geophys. J. R. Astron. Soc. 4 (1961) 276–281.
[2] S.I. Braginsky, P.H. Roberts, Equations governing convection in Earth's core and the geodynamo, Geophys. Astrophys. Fluid Dyn. 79 (1995) 1–97.
[3] S.I. Braginsky, Structure of the F layer and reasons for convection in the Earth's core, Dokl. Akad. Nauk SSSR 149 (1963) 8–10.
[4] D.E. Loper, A model of the dynamical structure of Earth's outer core, Phys. Earth Planet. Inter. 117 (2000) 179–196.
[5] D.E. Loper, Dynamo energetics and the structure of the outer core, Geophys. Astrophys. Fluid Dyn. 49 (1989) 213–219.
[6] J. Bloxham, A. Jackson, Fluid flow near the surface of Earth's outer core, Rev. Geophys. 29 (1991) 97–120.
[7] G.A. Glatzmaier, P.H. Roberts, A three-dimensional convective dynamo solution with rotating and finitely conducting inner core and mantle, Phys. Earth Planet. Inter. 91 (1995) 63–75.
[8] G.A. Glatzmaier, P.H. Roberts, An anelastic evolutionary geodynamo simulation driven by compositional and thermal convection, Physica D 97 (1996) 81–94.
[9] G.A. Glatzmaier, P.H. Roberts, Simulating the geodynamo, Contemp. Phys. 38 (1997) 269–288.
[10] Y. Ogura, N.A. Phillips, Scale analysis of deep and shallow convection in the atmosphere, J. Atmos. Sci. 19 (1962) 173–179.
[11] S.I. Braginsky, Magnetohydrodynamics of Earth's core, Geomag. Aeron. 4 (1964) 698–712.
[12] D.O. Gough, The anelastic approximation for thermal convection, J. Atmos. Sci. 26 (1969) 448–456.

[13] J. Latour, E.A. Spiegel, J. Toomre, J.-P. Zahn, Stellar convection theory I. The anelastic modal equations, Ap. J. 207 (1976) 233–243.
[14] P.A. Gilman, G.A. Glatzmaier, Compressible convection in a rotating spherical shell I. Anelastic equations, Ap. J. Suppl. 45 (1981) 335–349..
[15] T.M. Rogers, G.A. Glatzmaier, Penetrative convection within the anelastic approximation, Astrophys. J. 620 (2005) 432–441.
[16] S.V. Starchenko, M.S. Kotelnikova, Symmetric heat and mass transfer in a rotating spherical layer, J. Exp. Theor. Phys. 94 (2002) 459–469.
[17] D.V. Alexandrov, A.P. Malygin, Comments on article Symmetric heat and mass transfer in a rotating spherical layer, JETP 94 (3) (2002) 459 (J. Exp. Theor. Phys. 114 (2012) 257–258).
[18] D.V. Alexandrov, A.P. Malygin, Coupled convective and morphological instability of the inner core boundary of the Earth, Phys. Earth Planet. Int. 189 (2011) 134–141.
[19] M.G. Worster, Natural convection in a mushy layer, J. Fluid Mech. 224 (1991) 335–359.
[20] A.M. Dziewonski, D.L. Anderson, Preliminary reference Earth model, Phys. Earth Planet. Inter. 25 (1981) 297–356.
[21] A.P. Anufriev, C.A. Jones, A.M. Soward, The Boussinesq and anelastic liquid approximations for convection in the Earth's core, Phys. Earth Planet. Inter. 152 (2005) 163–190.
[22] A.P. Anufriev, I. Cupal, Characteristic amplitudes in the solution of the anelastic geodynamo model, Phys. Earth Planet. Inter. 124 (2001) 167–174.
[23] D.V. Alexandrov, Solidification with a quasiequilibrium mushy region: exact analytical solution of nonlinear model, J. Cryst. Growth 222 (2001) 816–821.
[24] D.V. Alexandrov, Solidification with a quasiequilibrium two-phase zone, Acta Mater. 49 (2001) 759–764.
[25] D.L. Aseev, D.V. Alexandrov, Directional solidification of binary melts with a non-equilibrium mushy layer, Int. J. Heat Mass Transfer 49 (2006) 4903–4909.
[26] D.L. Aseev, D.V. Alexandrov, Nonlinear dynamics for the solidification of binary melt with a nonequilibrium two-phase zone, Phys. Doklady 51 (2006) 291–295.
[27] M.G. Worster, J.S. Wettlaufer, Natural convection, solute trapping, and channel formation during solidification of saltwater, J. Phys. Chem. B. 101 (1997) 6132–6136.
[28] T.H. Solomon, R.R. Hartley, A. Lee, Aggregation and chimney formation during the solidification of ammonium chloride, Phys. Rev. E. 60 (1999) 3063–3071.
[29] R.F. Katz, M.G. Worster, Simulation of directional solidification, thermochemical convection, and chimney formation in a Hele-Shaw cell, J. Comput. Phys. 227 (2008) 9823–9840.
[30] D.R. Fearn, D.E. Loper, P.H. Roberts, Structure of the Earth's inner core, Nature 292 (1981) 232–233.
[31] Yu.A. Buyevich, D.V. Alexandrov, V.V. Mansurov, Macrokinetics of crystallization, Begell House Inc., New York, 2001.
[32] H. Shimizu, J.P. Poirier, J.L. Le Mouël, On crystallization at the inner core boundary, Phys. Earth Planet. Inter. 151 (2005) 37–51.
[33] D.E. Loper, P.H. Roberts, A study of conditions at the inner core boundary of the Earth, Phys. Earth Planet. Inter. 24 (1981) 302–307.
[34] M.I. Bergman, D.R. Fearn, Chimneys on the Earth's inner-outer core boundary?, Geophys Res. Lett. 21 (1994) 477–480.
[35] R. Deguen, T. Alboussière, D. Brito, On the existence and structure of a mush at the inner core boundary of the Earth, Phys. Earth Planet. Inter. 164 (2007) 36–49.
[36] P. Pelce, D. Bensimon, Theory of dendrite dynamics, Nucl. Phys. B. 2 (1987) 259–270.
[37] P. Pelce, Dynamics of Curved Fronts, Academic Press, Boston, 1988.
[38] D.A. Kessler, J. Koplik, H. Levine, Pattern selection in fingered growth phenomena, Adv. Phys. 37 (1988) 255–339.
[39] E.A. Brener, V.A. Mel'nikov, Pattern selection in two-dimensional dendritic growth, Adv. Phys. 40 (1991) 53–97.
[40] M. Benamar, Ph. Bouissou, P. Pelce, An exact solution for the shape of a crystal growing in a forced flow, J. Cryst. Growth 92 (1988) 97–100.
[41] Ph. Bouissou, P. Pelce, Effect of a forced flow on dendritic growth, Phys. Rev. A 40 (1989) 6673–6680.
[42] M. Ben Amar, P. Pelce, Impurity effect on dendritic growth, Phys. Rev. A 39 (1989) 4263–4269.
[43] Ph. Bouissou, B. Perrin, P. Tabeling, Influence of an external flow on dendritic crystal growth, Phys. Rev. A 40 (1989) 509–512.
[44] D.V. Alexandrov, P.K. Galenko, D.M. Herlach, Selection criterion for the growing dendritic tip in a non-isothermal binary system under forced convective flow, J. Cryst. Growth 312 (2010) 2122–2127.
[45] E. Scheil, Bemerkungen zur schichtkiistallbildung, Z. Metallkd. 34 (1942) 70–72.
[46] M.I. Bergman, Estimates of the Earth's inner core grain size, Geophys. Res. Lett. 25 (1998) 1593–1596.
[47] S.A. Morse, Adcumulus growth of the inner core, Geophys. Res. Lett. 13 (1986) 1466–1469.
[48] S.A. Morse, No mushy zones in the Earth's core, Geochim. Cosmochim. Acta 66 (2002) 2155–2165.